Diamond & Related Materials 20 (2011) 999–1004

Contents lists available at ScienceDirect

Diamond & Related Materials

journal homepage: www.elsevier.com/locate/diamond

Effect of tantalum nitride supporting layer on growth and morphology of carbon nanotubes by thermal chemical vapor deposition☆☆

B. Bouchet-Fabre [a,*], A. Fadjié-Djomkam [a,b], R. Fernandez-Pacheco [c,d], M. Delmas [a], M. Pinault [a], P. Jegou [e], C. Reynaud [a], M. Mayne-L'Hermite [a], O. Stephan [c], T. Minéa [b]

[a] Laboratoire Francis Perrin, DSM/IRAMIS/SPAM (CNRS-URA 2453), CEA-Saclay, 91191 Gif surYvette Cedex, France
[b] Laboratoire de Physique des Gaz et des Plasmas (CNRS-UMR 8578), Université Paris-Sud, Bat. 210, 91405 Orsay Cedex, France
[c] STEM Group- Laboratoire de Physique des Solides (CNRS-UMR 8502), Université Paris-Sud, Bat. 510, 91405 Orsay Cedex, France
[d] Instituto de Nanociencia de Aragón (LMA-INA), Universidad de Zaragoza, Edificio I+D, CampusRío Ebro, 50018 Zaragoza, Spain
[e] CEA/ DSM/IRAMIS/SPCSICEA-Saclay, 91191 Gif sur Yvette Cedex, France

ARTICLE INFO

Available online 14 May 2011

Keywords:
Carbon nanotubes
Chemical vapour deposition
Tantalum nitride
Raman
High resolution transmission electron microscopy
Barrier layer

ABSTRACT

The role of tantalum nitride (TaNx) thin films as buffer layers on the control of nucleation and growth of aligned carpet-like carbon nanotubes (CNTs) has been proved. TaNx thin films have been deposited on Si by controlled magnetron sputtering process. Multiwall CNTs have been synthesized at 850 °C using an aerosol of ferrocene diluted in toluene. Electron microscopy images show a strong correlation between the growth rate and morphology of the CNTs and the initial composition of the TaNx thin films. Multi-scale investigations reveal that both morphology and structure of the CNTs are determined by the properties of the TaNx films. Raman and X-ray photoelectron spectroscopy, high resolution TEM imaging at the submicrometric and atomic scales have been used to confirm these hypotheses.

© 2011 Published by Elsevier B.V.

1. Introduction

Because of their unique structure, carbon nanotubes (*CNTs*) are expected to lead to a significant breakthrough in the electronic and mechanical engineering of materials. In the latest years important scientific advances have taken place in the fabrication and the improvement of CNTs properties. Hitherto, several techniques have been developed for growing nanotubes, such as arc discharge, laser ablation, chemical vapor deposition (CVD), hot filament assisted CVD, and plasma enhanced CVD (PECVD)[1,2]. In particular the aerosol assisted CCVD [3–8] represents an effective technique for the production of aligned CNTs on substrates. Numerous studies have been devoted to the understanding of the CNTs growth by CCVD [9–11]. The model nowadays adopted describes the growth following three stages: (i) *decomposition* of the carbon precursor on the catalytic nanoparticles, (ii) *diffusion* of C atoms inside this particle, and (iii) *separation*, in which graphene cylinders precipitate at the surface of the catalytic particle [12]. Thus, the interaction between the catalytic particle and the substrate at the atomic scale would affect significantly the CNT growth. To check this, the growth of CNTs by CCVD has been tested on various materials. The growth process was found to be unfavorable on metals, ceramic or carbon fibers [13–17]. An alternative proposed issue is to uniformly coat the fiber or metal before the CCVD process [18–24]. However, the growth control on specific substrates has to be supported by an extended expertise on the mechanism involved in the nucleation growth of the CNTs. A recent and promising way is the use of a mastered barrier layer between the substrate and the CNTs, which interacts with the catalyst. The composition, nanostructure or the roughness of the layers are parameters to be controlled. With that aim we have applied an aerosol assisted CCVD process [9], on a set of tantalum nitride TaNx thin films [24]. The barrier role of pure tantalum thin films in the CNT growth for ultra large-scale integrated (ULSI) circuits has already been tested by Fujitsu company [25] and recent works have been reported on the role of diffusion barrier of pure Ta films against iron catalysts, for a rapid CNT growth by CVD [26,27]. Besides TaNx thin films are known to play the role of diffusion barrier in electronic devices [28]; they exhibit a great variety of nanostructures and properties associated to the amount of nitrogen [29,30]. For our purposes, TaNx films were produced by PVD process, which is a versatile method to control the nano-composition and the nanostructure of the films [31]. We have previously shown that multiwall CNT were grown on TaNx and emphasized the strong correlation observed between the CNT growth parameters (length, external diameter) and the initial composition of the TaNx thin films [24].

This paper studies the morphology and the structure at the nanometric scale of the CNTs grown on TaNx exploiting the results obtained by Scanning (SEM) and Transmission Electron Microscopy (TEM) techniques, and by Raman and X-Ray photoelectron spectroscopy. In particular the interface between the inner iron nanowires and

☆☆ Presented at the Diamond 2010, 21st European Conference on Diamond, Diamond- Like Materials, Carbon Nanotubes, and Nitrides, Budapest.

* Corresponding author.
E-mail address: Brigitte.bouchet-fabre@cea.fr (B. Bouchet-Fabre).

0925-9635/$ – see front matter © 2011 Published by Elsevier B.V.
doi:10.1016/j.diamond.2011.05.006

the graphene layers of the CNTs were investigated by High Resolution TEM imaging at the atomic scale, whereas the cristallinity and chemical composition of the nanowires were studied by means of the analysis of the diffractograms resulting from the TEM images.

2. Experimental

2.1. The synthesis

The CNTs were grown on the TaNx coated Si, by aerosol assisted CCVD at 850 °C [9,32]. The aerosol, composed of ferrocene diluted in toluene at 2.5 wt.%, was generated by an injection system (Qualiflow-Jipelec Comp., France) coupled with an evaporator maintained at 200 °C and dragged into the reactor by Ar (3 L/mn). The deposition duration was fixed at 12 min. At the end of the experiment, the samples were slowly cooled down to room temperature before analysis. The set of TaNx thin films chosen for the nanotube growth were deposited on silicon by conventional radio frequency (RF: 400 W) magnetron sputtering (AC450) in reactive plasma N2/Ar with Ta target at 0.5 Pa. The Ar flow rate was fixed at 100 sccm while the N2 flow rate was varied from 0 to 20 sccm. The film thickness is about 130 nm. As reported in Table 1, the atomic ratio [N]/[Ta] in pristine thin films extends from 0.3 for 1sccm N2 in 100 sccm Ar, to 1.8 for 18 sccm N2 mixed to 100 sccm Ar, as determined by XPS with a two layers model [31]. The characteristics of the buffers and carpet nanotubes are summarized in Table 1.

2.2. Electron microscopy

Morphology and thickness of the CNT carpets were investigated by SEM (Leo Gemini1525, field-emission gun or Jeol JSM 6060 LV). TEM samples were prepared by suspending CNTs in ethanol. After sonication of the suspension a droplet of the supernatant was deposited on a Lacey Carbon TEM copper grid. TEM images of the CNTs were obtained in a TEM (Philips CM 12) at low magnification, for a statistical analysis of the external CNT diameters. HRTEM results were obtained using an image aberration corrected FEI TITAN at 60 kV, with a FEG extraction voltage of 2100 V. Correction of the spherical aberration of the objective lens leads to a spatial resolution closer to 0.1 nm.

2.3. Raman spectroscopy and XPS analysis

Carbon structures were analyzed by Raman spectroscopy at 532 nm (Renishaw Invia Reflex). The chemical composition of the CNTs and the TaNx thin films before and after the growth of CNTs were checked in a KRATOS AXIS UltraDLD, using a spot of $700 \times 300\ \mu^2$ from a monochromatised source (Al Kα 1486.6 eV). The core levels (Fe2p, Ta4f, C1s, N1s, O1s) were recorded with an analyzer operating at 20 eV for an energy resolution of 0.2 eV, in floating configuration with charge compensation. The energy was calibrated with a gold film deposited on glass.

Table 1
Principal characteristics of the set of buffer layers deduced from diffraction and XPS analysis [31] and characteristics of the CNT carpets extracted from XPS.

Sample		S1	S2	S3	S4	S5	S6
TaN buffer characteristics							
Buffer name		TaN_1	TaN_2	TaN_5	TaN_{10}	TaN_{16}	TaN_{18}
Plasma condition	N_2:Ar	1:100	2:100	5:100	10:100	16:100	18:100
Crystalline phases		α-Ta(N)	α-Ta(N)	TaN Ta_2N	TaN Ta_5N_6	TaN Ta_5N_6	TaN Ta_5N_6
N/Ta extracted from XPS		0.28	0.55	1.2	1.55	1.65	1.75
O/Ta (at the surface)		2.45	2.39	1.88	1.58	1.51	1.31
CNT carpet							
Csp^3/Csp^2+Csp^3		0.27	0.31	0.32	0.29	0.27	0.28
C-Fe bonding upon the carpet	At.%	3.1	3.3	2.5	3.8	2.4	2.1
[Fe]/[C] by XPS upon the carpet	At.	3.2	2.7	4.4	2.5	3.6	2.3
[O]/[Fe] by XPS upon the carpet	At.	1.8	1.5	2.1	1.8	1.6	1.9

3. Results and discussion

3.1. CNT carpet morphology

Fig. 1 shows the CNT growth product imaged by SEM for S2, S3 and S5 (Table 1). All the samples were placed in the isotherm zone of the furnace where the CNT growth is uniform [32]. Clean multiwall CNTs carpets were obtained, and a decrease of the growth rate was observed as the amount of nitrogen increased in the buffer films [24]. For the lowest N amount (S1), we obtained well aligned CNTs with a length about 150 μm for a 12 min. process. Conversely, for the highest N amount (S5–S6), a discontinuity in the coating of the buffer by the CNTs was observed, with a reduced CNT length of about 40 ± 10 μm and a loss of the alignment. As observed by TEM (Fig. 2) conventional multiwall CNTs were produced on TaNx buffers, with hollow core partially filled with iron based nanowires and nanoparticles. We also observed that their external diameter decreases when the nitrogen amount increases in the buffer [24]. The percentile d50 reaches typically 80 nm for S1 and gets down to 35 nm for S5, in comparison to 40 nm for CNTs grown on silicon. The longer the CNTs are, the larger their external diameter is. The properties of the CNTs carpet depend on both: the synthesis parameters and the buffer characteristics. It has been shown that the carpet length decreases greatly with increasing Ar flux [33,34]. Thus, the length of S1 may be compared to the 400 μm obtained for a carpet grown on thick SiO_2 film (400 nm) with an Ar flux of 1 l/mn [19]. We may conclude that first the CNTs grown on the solid solution α-Ta(N) (e.g. S1, S2) have large external diameters and the typical growth rate known for our CCVD process. Conversely, as the amount of nitrogen of the buffer increases, near or above the TaN stoichiometry, the growth of CNTs is delayed and/or slowed down.

3.2. The carbon walls

Fig. 3 is a summary of the carbon walls XPS characterization, showing the core level details of C1s and N1s, associated to a HRTEM local image of the nanotubes (inset). As confirmed by HRTEM, the multiwall CNTs have diameters between 60 and 150 nm and the iron based nanowires filling them have up to several tens of nanometers long. Even though some of them were cut or divided in several pieces during TEM specimen preparation, most of the tubes were complete and well isolated from each other. Depending on the concentration of nitrogen in the buffer, the shape of tubes slightly changes, being more irregular for lower ratios N/Ta. For lower concentrations of nitrogen (S1–S3), irregular, helicoidally or chain-shaped tubes seem to be more frequent, whereas for higher amounts of nitrogen incorporated into the buffer layer (S5–S6) CNTs tended to be more straight and homogeneous. In those cases perfect equidistant graphitic walls were observed with typical distances of 0.37 nm between carbon walls and 0.24 nm between graphitic sheets for the same wall.

Concerning XPS spectra, there is no significant change in the C1s core level taken upon the CNTs carpets when the amount of nitrogen increases in the buffers. The C1s core levels are narrow (FWHM .55 eV), with a maximum located at 284.1 eV; this energy is lower than the value for Csp^2 (284.5 eV) in graphite, but such low values have been already observed in MWCNTs [35,36] and freestanding graphene layers [37]; it may be indicative of the bad conduction at the interface between the CNTs and the buffers. Considering a shift of −0.3 eV of the overall spectra, the decomposition of the asymmetric

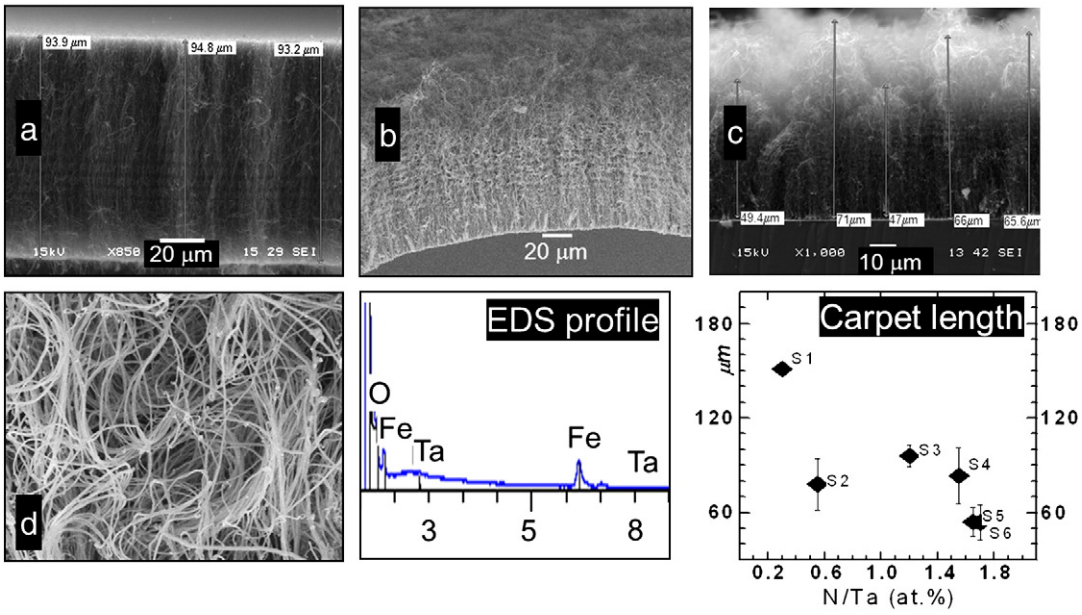

Fig. 1. SEM image of the aligned NTs carpet for S2 (a), S3 (b) and S5(c), produced by aerosol assisted CCVD process using ferrocene in toluene at 850 °C. Picture (d) focuses on a typical top of a carpet (S3). A typical EDS profile is also shown and the average carpet length after 12 mn growth is presented for the set of samples, as a function of N/Ta (extracted from XPS).

core level has been done in four symmetric components, namely the Csp^2 (here 284.1 eV), the Csp^3 component (284.7, FWHM .95 eV), the carbon bonding with a heteroatom, O or N (285.8 eV, FWHM 1.5 eV), and C bonded to Fe at the interface with metallic nanowires (283.3 eV, FWHM .5 eV). The contribution of the component Csp^3 generated by the curvature of the walls, local defects and charge transfer is small. The ratio $Csp^3/(Csp^2+Csp^3)$ reported in Table 1, oscillates around 27–32%, with a maximum for S3. The bonding with a heteroatom (O,

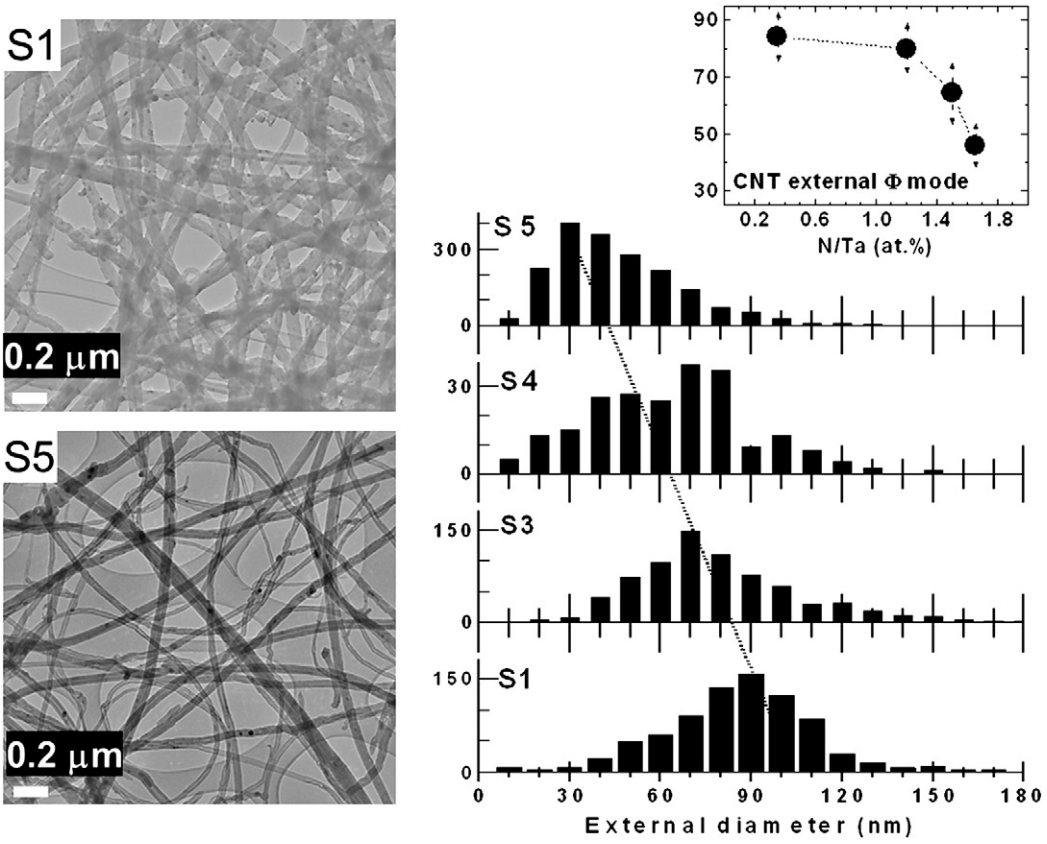

Fig. 2. Typical TEM image of the CNTs carpet for S1 and S5, produced by aerosol assisted CCVD process using ferrocene in toluene at 850 °C and evolution of the diameters for S1, S3, S4 and S5. The inset represents the evolution of the mode for the given set of samples, as a function of N/Ta extracted from XPS.

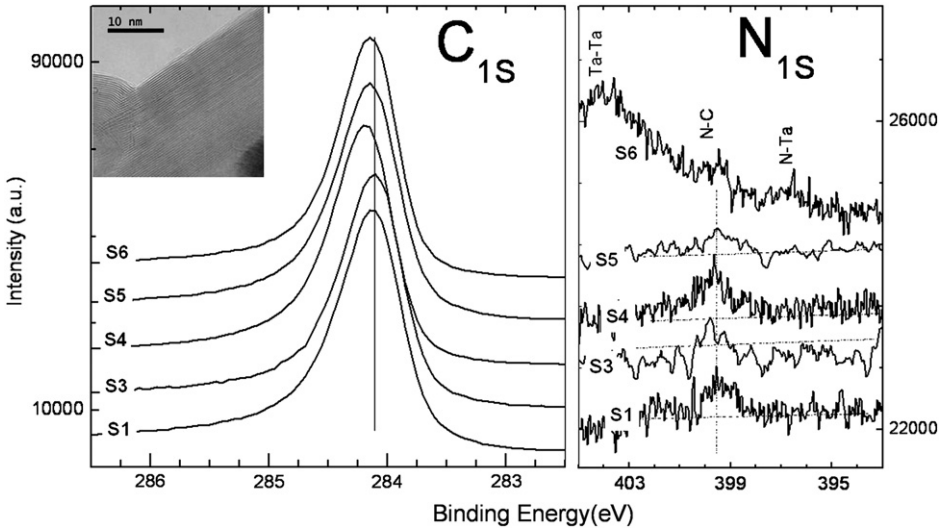

Fig. 3. C_{1s} and N_{1s} core level for the set of samples S1, S3, S4, S5 and S6, associated to typical local image of the CNTs layer as it may be done by HRTEM (inset).

N) and Fe represents respectively 6–8% and 2–4% of the signal. Fig. 4 presents the Raman spectra for the set of samples, for the D and G peak region and its harmonic (2D peaks). The D peak represents the collective breathing mode due to aromatic rings, while the G peak is due to the C–C stretching mode from all sp^2 structures [38]. The Raman spectra are then indicative of the order in the walls for the MWCNTs [39].

Main lines have a Lorentz shape. When the amount of nitrogen in the buffer increases, the G peak width decreases from 38 cm^{-1} to 31 cm^{-1} while its energy shift from 1586.7 to 1585.7 cm^{-1}. The large width and energy are due to the disorder in the carbon layers: for HOPG, the width would be 13 cm^{-1} and the G peak centered on 1582 cm^{-1}. The decrease of both values indicates that an increase of the amount of nitrogen is correlated to an improving of the cristallinity of the nanotubes walls. The vibration mode D_2 at 1610 cm^{-1} is usually connected to boundary background modes induced by the small sizes of the carbon nano-clusters. The I_D/I_G and I_{2D}/I_D ratios, which conventionally indicate the degree of order in the clustered aromatic sp^2 phase in carbon materials, are presented in the inset: the first decreases from 0.8 (for S2) to 0.5 (for S5–S6). The latter oscillates reaching 4 for stoichiometric N/Ta buffer. However, according to Tuinstra and Koeni, the variation of I_D/I_G corresponds to the increase of a vibration mean coherence length from 60 nm to 100 nm [39]. These results are in agreement with HRTEM local observations.

The bonding of carbon with a heteroatom at the interface with metallic nanowires, namely Fe (centered at 283.4 eV) and O (around 286.1 eV) represents respectively 2–4% and 4–6% of the signal. The N1s core level shows a very small signal around 399.8 eV, of very few isolated nitrogen bonded to sp^2 carbon (2 at.‰). This indicates that a part of nitrogen constituting the TaNx buffers contribute to the atomic exchanges during the CNT growth. The N1s core level for S6 is slightly different: the CNTs do not cover the buffer and then it represents the addition of two environments, one coming from N bonded to C in the CNTs and a second one coming from the buffer (superposition of. Ta4p

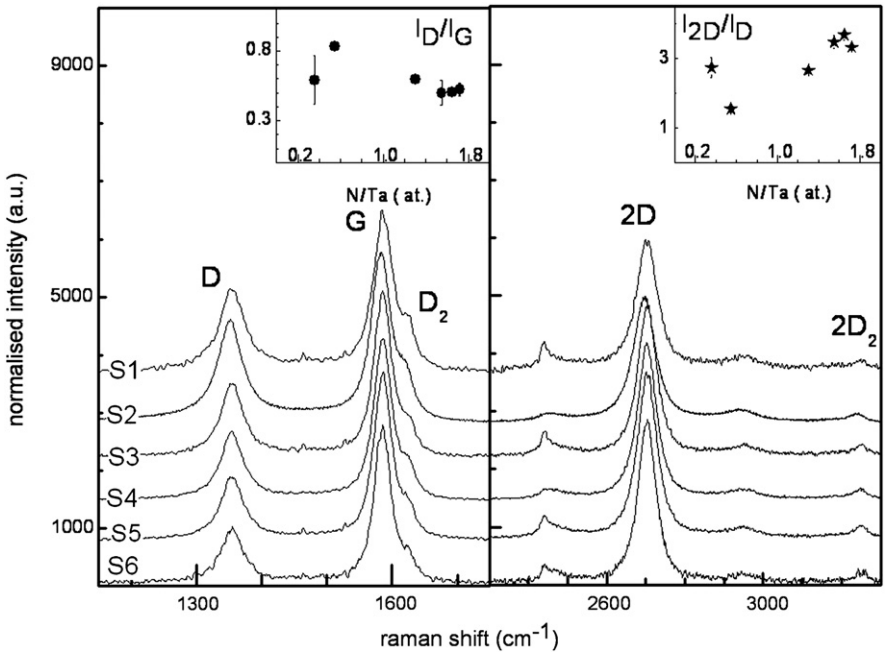

Fig. 4. Raman spectra for the set of CNTs samples produced by aerosol assisted CCVD process using ferrocene in toluene at 850 °C. The ratios I_D/I_G and I_{2D}/I_D shown in the inset have been deduced from a Lorentzian decomposition of the peaks.

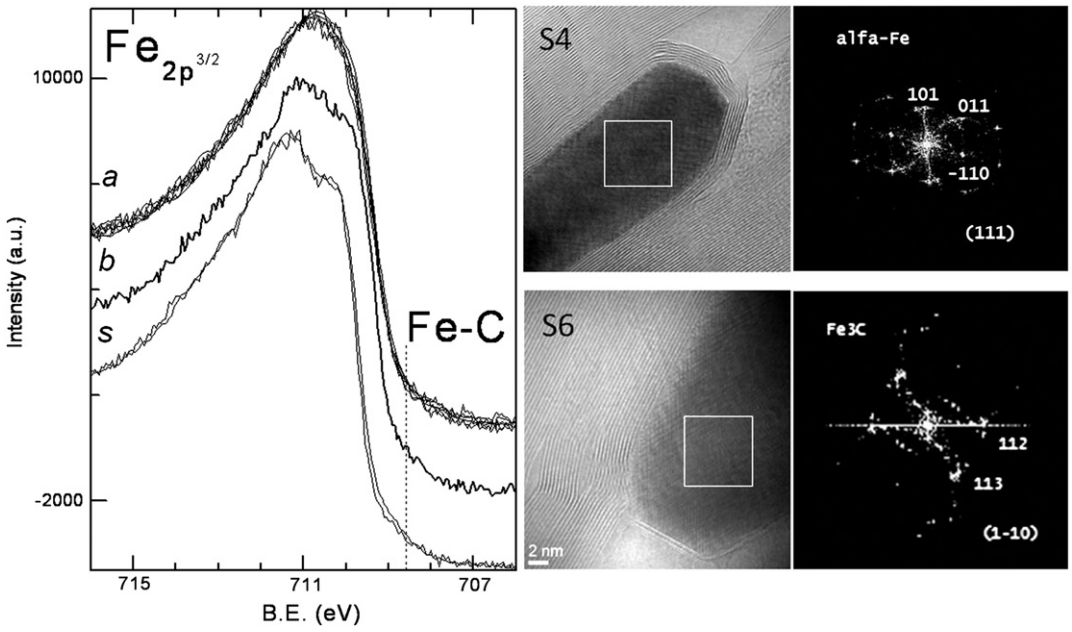

Fig. 5. Metallic nanowires and nanoparticles: the $Fe_{2p}^{3/2}$ core level taken on the CNTs carpet, on the top of the carpets for the set of samples (*a*), at the bottom of the CNTs for S1 (*b*) and on the substrate (*s*) after removing most of the carpet for S1–S2. The HRTEM pictures show typical thin nanowires inside a CNT and their diffractograms.

centered on 407–408 eV and the core levels of N bonded to Ta between 395 eV and 398 eV).

3.3. Iron based nanoparticles

Fig. 5a shows the core level details of $Fe_{2p}^{3/2}$ taken at the top (a), the bottom for S1–S2 (b) of the CNTs carpet and also on the buffer surface after removing the CNTs for S1–S2–S3 (s). The Ta4f core level record and the EDS measurements performed on the top of the CNT carpet (not shown) proves that there is no Ta inside the nanowires confined in the CNTs. The inset shows a typical nanowire inside a CNT and the buffer surface after removing the CNTs. The $Fe_{2p}^{3/2}$ core level coming from the nanowires at the top or at the bottom of the carpet, are independent of the pristine TaNx buffers nature: they all may be considered as the addition of 3 main components. The two larger contributions (FWHM 2.3 eV) respectively at 711.1±.3 eV and 712.9±0.2 eV, may be assigned to Fe^{2+} and Fe^{3+}, in a Fe_3O_4-type surrounding [40]. They represent 76% of the signal at the top of all the carpet, increase up to 79% at the bottom and 83–88% on the buffer surface. The third contribution is thinner (FWHM 1.2 eV) and located at 709.8±0.2 eV: it corresponds to Fe—O type surrounding; it represents respectively 23% and 17% of the signal at the top and bottom of the CNTs carpet. At the interface CNT-buffer, it decreases from 15% to 11% from S1 to S3. Only 2% of the core level at the top and 4% at the bottom of the CNT may be attributed to metallic iron, centered on 707.9±0.2 eV, which correspond to Fe—C bonding in accordance with the carbon surrounding.

By HRTEM we have explored the nanowires of small diameter as shown in Fig. 5b. Applying the Fast Fourier Transform to each image we can obtain the power spectrum of the real image. In that way we obtain diffractograms for each iron-based particle, equivalent to the diffraction pattern we would obtain by electron diffraction. If the particles are randomly oriented in a proper direction, i.e. with a zone axis parallel to the optic axis of the microscope, from the electron diffraction pattern, and by measuring distances and angles between spots we can discern between different crystalline structures. Thus, from the diffractograms of the different samples we found that most of the thin nanowires are crystallized in the phase of cementite (Fe_3C) or α-Fe (bcc). For each sample and for any initial concentration of nitrogen in the buffer we found tubes filled with nanowires and nanowires crystallized in both phases (Fig. 4). We have especially focused on the relation between iron and graphitic planes at the interface between particles and nanotubes. No specific epitaxial relationship has been found and angles between iron and carbon planes at the interface do not seem to follow any pattern. There is an apparent contradiction between the XPS results, which showed mostly oxide at the surface of the particles, and HRTEM observations, which showed that most of the nanowires crystallized as cementite or alpha-iron. This may be due on one side to the fact that XPS does not measure the core levels in the nanowires, too deeply embedded in the carbon multiwall; however this technique is sensitive to the surface of the nanoparticles poorly covered by graphite layers, even if they are scarce, as seen by SEM. On the other side, HRTEM observations have been made on a restricted number of nanowires, and may not be done for too thick nanowires or nanoparticles, since they would not be transparent to the electron beam.

4. Conclusion

Aligned carbon nanotubes have been grown by assisted aerosol CCVD process on a set of TaNx buffers. We have shown the strong influence of TaNx buffers on the CNTs geometry and growth rate. It has been observed that tantalum atoms remain at the interface CNT-buffer while nitrogen atoms leave the buffer, being present in the nanotubes. We have shown that as the amount of nitrogen in the buffer increases, the CNTs cristallinity increases, whereas the diameter of the nanotubes and their growth rate decrease. Despite these evolutions, the local surrounding of carbon atoms seems constant and most of the nanowires confined in CNTs are crystallized in cementite or alpha-iron phase, while bigger particles are coated by iron oxide.

Acknowledgements

C. Jin, M.C. Hugon and O. Antonin (LPGP, UMR 8578) are acknowledged for the production and analysis of the TaNx buffers. C. Bertier, S. Poissonnet and P. Bonnaillie (CEA-Saclay DEN/SRMP) are acknowledged for SEM observations. Prof. F. Alvarez (Campinas, Brazil) is very kindly acknowledged for the helpful scientific discussion.

References

[1] M. Meyyappan, L. Delzeit, A. Cassell, D. Hash, Plasma Sources Sci. Technol. 12 (2003) 205.
[2] A. Gohier, T.M. Minea, A.M. Djouadi, A. Granier, M. Dubosc, Chem. Phys. Lett. 421 (2006) 242.
[3] R. Andrews, D. Jacques, A.M. Rao, F. Derbyshire, D. Qian, X. Fan, E.C. Dickey, J. Chen, Chem. Phys. Lett. 303 (1999) 467.
[4] R. Kamalakaran, M. Terrones, T. Seeger, P. Kohler-Redlich, M. Rühle, Y.A. Kim, T. Hayashi, M. Endo, Appl. Phys. Lett. 77 (2000) 3385.
[5] M. Mayne, N. Grobert, M. Terrones, R. Kamalakaran, M. Rühle, H.W. Kroto, D.R.M. Walton, Chem. Phys. Lett. 338 (2001) 101.
[6] C. Singh, M.S.P. Shaffer, K.K.K. Koziol, I.A. Kinloch, A.H. Windle, Chem. Phys. Lett. 372 (2003) 860.
[7] Z.J. Zhang, B.Q. Wei, G. Ramanath, P.M. Ajayan, Appl. Phys. Lett. 77 (2000) 3764–3766.
[8] M. Pinault, V. Pichot, H. Khodja, P. Launois, C. Reynaud, M. Mayne-L'Hermite, Nanoletters 5 (2005) 2394.
[9] M. Pinault, M. Mayne-L'Hermite, C. Reynaud, V. Pichot, P. Launois, D. Ballutaud, Carbon 43 (2005) 2968.
[10] A. Oya, H. Marsh, J. Mater. Sci. 17 (1982) 309.
[11] S.A. Moshkalev, C. Verissimo, J. Appl. Phys. 102 (2007) 044303.
[12] O.V. Yazyev, A. Pasquarello, Phys. Stat. Solid B 245 (2008) 2185.
[13] L.T. Qu, Y. Zhao, L.M. Dai, Small 2 (2006) 1052.
[14] W.Z. Li, D.Z. Wang, S.X. Yang, J.G. Wen, Z.F. Ren, Chem. Phys. Lett. 335 (2001) 141.
[15] R.B. Mathur, S. Chatterjee, B.P. Singh, Compos. Sci. Technol. 68 (2008) 1608.
[16] Z.G. Zhao, L.J. Ci, H.M. Cheng, J.B. Bai, Carbon 43 (2005) 663.
[17] N. Yamamoto, A.J. Hart, E.J. Garcia, S.S. Wicks, H.M. Duong, A.H. Slocum, B. Wardle, Carbon 47 (2009) 551.
[18] J. Garcia-Cespedes, S. Thomasson, K.B.K. Teo, I.A. Kinloch, W.I. Milne, E. Pascual, E. Bertran, Carbon 47 (2009) 613.
[19] M. Delmas, M. Pinault, D. Porterat, C. Reynaud, M. Mayne-L'Hermite, Proceeding, Euro CVD17 (Vienne, 4–9 October 2009), 2009.
[20] H.C. Iee, P.S. Alegaonkar, D.Y. Kim, J.H. Lee, T.Y. Lee, S.Y. Jeon, J.B. Yoo, Thin Solid Films 516 (2008) 3646.
[21] J.W. Ward, B.Q. Wei, P.M. Ajayan, Chem. Phys. Lett. 376 (2003) 717.
[22] Hou T. Ng, B. Chen, J.E. Koehne, A. Cassell, J. Li, J. han, M. Meyyappan, J. Phys. Chem. B 107 (2003) 8484.
[23] R.V. Pulikollu, S.M. Mukhopadhyay, Appl. Surf. Sci. 253 (2007) 7342.
[24] B. Bouchet-Fabre, A. Fadjie-Djomkam, M. Delmas, C. Jin, O. Antonin, M.C. Hugon, M. Mayne-L'Hermite, F. Alvarez, T. Minéa, Carbon 47 (2009) 3424.
[25] M. Horibe, M. Nihei, D. Kondo, A. Kawabata, Y. Awano, Jpn. J. Appl. Phys. 44 (2005) 5309.
[26] Y. Wang, Z. Luo, B. Li, P.S. Ho, Z. Yao, L. Shi, Appl. Phys. Lett. 89 (2006) 183113.
[27] Y. Wang, Z. Luo, B. Li, P.S. Ho, Z. Yao, L. Shi, E.N. Bryan, R.J. Nemanich, J. Appl. Phys. 101 (2007) 124310.
[28] E. Machado, M. Kaczmarski, P. Ordejn, D. Garg, J. Norman, H. Cheng, Langmuir 21 (2005) 7608.
[29] T. Riekkinen, J. Molarius, T. Laurila, A. Nurmela, I. Suni, J.K. Kivilahti, Microelectron. Eng. 64 (2002) 289.
[30] T.C. Li, B.J. Lwo, N.W. Pu, S.P. Yu, C.H. Kao, Surf. Coat. Technol. 201 (2006) 1031–1036.
[31] C. Jin, M. Delmas, P. Aubert, F. Alvarez, T. Minéa, M.C. Hugon, B. Bouchet-Fabre, Thin Solid Films 519 (2011) 4097.
[32] M. Pinault, M. Mayne-L'Hermite, C. Reynaud, O. Beyssac, J.N. Rouzaud, C. Clinard, Diam. Relat. Mater. 13 (2004) 1266.
[33] C. Castro, PhD thesis, Orsay (2009), in French.
[34] C. Castro, M. Pinault, S. Coste-Leconte, D. Porterat, N. Bendiab, C. Reynaud, M. Mayne-L'Hermite, Carbon 48 (2010) 3807–3816.
[35] S. Suzuki, Y. Watanabe, S. Heun, Curr. Opin. Solid State Mater. Sci. 10 (2006) 53.
[36] S. Mathew, U.M. Bhatta, J. Ghatak, B.R. Sekhar, B.N. Dev, Carbon 45 (2007) 2659.
[37] S. Lizzit, A. Baraldi, Catal. Today 154 (2010) 68.
[38] A.C. Ferrari, J. Robertson, Phys. Rev. B 61 (2000) 14095.
[39] A.C. Ferrari, Solid State Commun. 143 (2007) 47.
[40] W. Xia, X. Chen, S. Kundu, X. Wang, G. Grundmeier, Y. Wang, M. Bron, W. Schuhmann, M. Muhler, Surf. Coat. Technol. 201 (2007) 9232.